Modeling the propagation of hydraulic fractures in reservoirs with natural fracture networks using high aspect ratio interface elements

Lucas G. Barbosa[1], Pedro R. Cleto[1], Murilo Camargo[2], Osvaldo L. Manzoli[1]

[1]*Dept. of Civil and Environment Engineering, São Paulo State University (UNESP)*
Av. Eng. Luiz Edmundo Carrijo Coube, 14-01, 17033-360, São Paulo, Brazil
lucas.guarnieri@unesp.br, pedro.cleto@unesp.br, osvaldo.l.manzoli@unesp.br
[2]*Dept. of Mechanical Engineering, São Paulo State University (UNESP)*
Av. Eng. Luiz Edmundo Carrijo Coube, 14-01, 17033-360, São Paulo, Brazil
murilo.camargo@unesp.br

Abstract. Hydraulic fracturing in unconventional reservoirs is a common technique used to overcome the problem of low permeability in porous media. However, understanding this method involves complex factors, such as the influence of in situ stress and the characteristics of natural fractures, including their lengths, angles, and aperture values. Thus, based on the continuum mechanics and using the finite element method, this paper seeks to simulate the effect of hydraulic fracturing in porous media with a complex network of natural fractures for different fluid injection rates. The modeling of the problem considers a fully coupled approach to solve the hydro-mechanical problem, with Darcy's law governing fluid flow in the porous media and the classical cubic law inside the fractures. High Aspect Ratio Interface Finite Elements (HAR-IEs) with a suitable tensile damage model represent natural and hydraulic fractures, inserted into the regular mesh via the Mesh Fragmentation Technique (MFT). The results are validated with the literature and demonstrate that the model effectively reproduces the complex scenarios of propagation and interaction between multiple fractures.

Keywords: Natural fracture networks, High aspect ratio interface elements, Hydro-mechanical analysis.

1 Introduction

The hydraulic fracturing technique consists of injecting a fluid under high pressure to overcome the problem of low permeability in reservoir rocks. Widely used by the oil and gas industry, the propagation of hydraulic fractures (HF) facilitates the extraction of resources from reservoir rocks by improving connectivity between the well and the rock matrix [1, 2].

Analytical studies developed in two-dimensional scenarios using the classic KGD (Kristianovich-Geertsma-de-Klerk) [3, 4] and PKN (Perkins, Kern and Nordgren) [5] models contribute to preliminary studies, but are not capable of incorporating all the parameters necessary for a more in-depth study of the application of the hydraulic fracturing technique [6]. The propagation of HFs can be impacted by a number of factors not considered in these models, such as the propagation of the multiple fractures and the distribution of a complex network of natural fractures (NFs) [6]. In this respect, naturally fractured porous media show that NFs also play a fundamental role in the behavior of HF in the porous medium, where various scenarios of interactions between fractures can be obtained according to the parameters of the rock [7].

To overcome the limitations of analytical approaches, experimental tests [8, 9] and numerical models capable of considering complex scenarios have emerged. In the context of numerical models, using the discrete element method, Zou et al. [10] verified the impact of different in situ stress states on the propagation of HF in a naturally fractured porous medium, showing that with a gradual increase in the difference between the stresses, the direction of HF propagation tends to be perpendicular to the lowest in situ stress. On the other hand, in the case of an isotropic stress state, the HF has no preferential direction. Wang [11] used cohesive zone model to simulate the impact of the NF network on HF propagation in cases with isotropic or slightly orthotropic stress states to study the stress shadow effect, where only one path tends to prevail and continue propagating even with the activation of nearby NFs. The finite element method was used by Wang et al. [12] to simulate a shale reservoir and observed that different properties of the NFs and stress states govern the propagation of HF.

Considering the finite element method, this paper evaluates the impact of a network of NFs on HF propagation

in a 2D scenario for an isotropic stress state and different fluid injection rates. High aspect ratio interface elements (HAR-IEs) [13] associated with a tensile damage law are used to represent fracture behavior. The fluid flow in the fracture is governed by the classical cubic law.

2 High aspect ratio interface element

High aspect ratio interface elements, proposed by Manzoli et al. [14] and based on the Continuous Strong Discontinuity Approach (CSDA) Oliver [15], are solid finite elements that can be used associated with conventional constitutive models to represent an approximation of the kinematics of discontinuities. Their characteristic high aspect ratio is given by the fact that their base is about 100 times larger than their height [13].

HAR-IEs have already been implemented in two-dimensional problems involving the propagation of fractures in porous media [13]. The advantages of using HAR-IEs show that (i) it is not necessary to use tracking algorithms; (ii) artificial parameters related to stiffness or (iii) pre-definition of crack path, where also (iv) it does not require techniques beyond the continuous laws already used in the rest of the problem [16], which allows the propagation of multiple fractures freely.

Assuming a tensile damage model, the fracture propagation is associated with the non-linear behavior of the HAR-IEs, which is initiated only when the damage criterion of the HAR-IE is reached. In the hydraulic problem, the fracture energy, i.e. the energy for fracture propagation to occur, is associated with the thickness h of the interface element, which is also included in the fracture mechanics formulation itself. Figure 1 illustrates the HAR-IE element of height h and base b, with the normal vector $\mathbf{n}$ to its base.
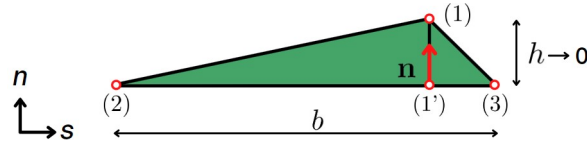
Figure 1. High Aspect Ratio Interface Element.

The strain and pressure fields for the HAR-IEs can be written, respectively, as [13]:

$$\boldsymbol{\epsilon} = \tilde{\boldsymbol{\epsilon}} + \hat{\boldsymbol{\epsilon}} = \tilde{\boldsymbol{\epsilon}} + \frac{1}{h}\left(\mathbf{n} \otimes [\![\mathbf{u}]\!]\right)^{sym}, \tag{1}$$

$$\boldsymbol{\nabla} p = \boldsymbol{\nabla}\tilde{p} + \boldsymbol{\nabla}\hat{p} = \boldsymbol{\nabla}\tilde{p} + \frac{1}{h}[\![p]\!]\mathbf{n}, \tag{2}$$

where $\tilde{\boldsymbol{\epsilon}}$ and $\boldsymbol{\nabla}\tilde{p}$ are the counterpart of the continuous strain tensor and the pressure gradient, respectively, which do not depend on the height h; $[\![\mathbf{u}]\!]$ and $[\![p]\!]$ are the relative displacement and pressure, respectively, between the node (1) and its projection (1'); $(\bullet)^{sym}$ is the symmetric part of $(\bullet)$ and $\otimes$ is the dyadic product.

Note that in the situation with $h \to 0$, node (1) tends to its respective projection (1'), which coincides for the same material point. Observe that the parameter h integrates the constitutive relations, which ensures the effect of energy dissipation and fracture formation. Thus, the jumps in displacement and pressure correspond to measurements of the discontinuity in the corresponding fields, i.e. the relative displacement and relative pressure.

2.1 Mesh Fragmentation Technique

The Mesh Fragmentation Technique (Fig. 2) is used to insert the HAR-IEs into the regular finite element mesh [17]. This technique consists of creating small gaps of size h between the finite elements of the regular mesh, a space where the HAR-IEs are inserted in pairs. Note that this dimension h coincides with the height of the HAR-IEs, and once inserted, they become part of the modeling of the porous medium.

3 Governing equation

Consider a domain Ω and boundary Γ, with the subdomains for the continuous part as Ω^c and discontinuous Ω^h, defining $\Omega = \Omega^c \cup \Omega^h$.
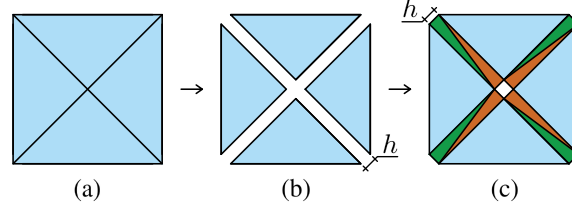
Figure 2. Process of the Mesh Fragmentation Technique: (a) regular mesh, (b) creation of the h dimension space between the elements and (c) the insertion of HAR-IEs pairs into the regular mesh.

3.1 Mechanical

Neglecting the effects of inertia, the momentum balance equation of the porous medium is given by [13]:

$$\boldsymbol{\nabla}{\cdot}(\boldsymbol{\sigma}' - bp\mathbf{1}) + \rho\mathbf{g} = 0, \tag{3}$$

where $\boldsymbol{\sigma}'$ is the effective stress tensor which can be described as a function of the constitutive model related to the continuous medium ($\boldsymbol{\Sigma}_{\Omega^c}(\boldsymbol{\epsilon}) = \bar{\boldsymbol{\sigma}} = \mathbb{C} : \boldsymbol{\epsilon}$, where $\mathbb{C}$ is the fourth order elastic tensor and $\boldsymbol{\epsilon}$ the strain tensor) and the discontinuity ($\boldsymbol{\Sigma}_{\Omega^h}(\boldsymbol{\epsilon})$), b is the Biot's coefficient also related to the continuous medium ($b_{\Omega^c} = 1 - K/K_s$, where K and Ks are the bulk moduli of the porous medium and of the solid phase, respectively) and the discontinuity (b_{Ω^h}), p is the pressure, $\mathbf{1}$ is the second-order identity tensor, ρ is the density of the fluid-matrix mixture and $\mathbf{g}$ is the vector of acceleration due to gravity.

3.2 Hydraulic

Under the assumption of a deformable porous medium and isothermal conditions, the fluid mass balance can be written, disregarding the source term, as follows [13]:

$$\frac{\dot{p}}{M} + b\nabla \cdot \dot{\mathbf{u}} + \nabla \cdot \mathbf{q} = 0, \tag{4}$$

where M is the Biot's modulus that can be written for the continuous domain ($M_{\Omega^c} = [\phi/K_w + (b - \phi)/K_s]^{-1}$, where K_w is the bulk modulus of the fluid) and discontinuous one (M_{Ω^h}), ϕ is the rock porosity that also can be written for the continuous domain ($\phi_{\Omega^c} = \phi_0$, where ϕ_0 is a constant) and the discontinuous one (ϕ_{Ω^h}), $\nabla \cdot \mathbf{u} = \epsilon_v$ is the volumetric strain and $\mathbf{q}$ is the fluid flow governed by Darcy's law, as follows:

$$\mathbf{q} = -\frac{\mathbf{k}}{\mu}(\boldsymbol{\nabla}p - \rho_l\mathbf{g}) \tag{5}$$

where μ is the dynamic viscosity of the fluid, ρ_l the fluid density and $\mathbf{k}$ can be written for the continuous domain ($\mathbf{k}_{\Omega^c} = \mathbf{k}_0$, where $\mathbf{k}_0$ is the intrinsic permeability tensor of the porous medium) and discontinuous one ($\mathbf{k}_{\Omega^h}$).

3.3 Initial and boundary conditions

The following initial and boundary conditions taken for the material points $\mathbf{X}$ and time t is shown in Table 1. Note that $\mathbf{u}_0$ and p_0 represents the initial displacement and the initial pressure, respectively, while $\bar{\mathbf{u}}$ and $\bar{p}$ is the prescribed displacement and pressure on the boundary Γ_u and Γ_p, respectively, $\bar{\mathbf{t}}$ are stresses imposed on the boundary Γ_t and $\bar{q}$ are flows imposed on boundary Γ_q. Thus, $\Gamma = \Gamma_u \cup \Gamma_t$ and $\Gamma = \Gamma_p \cup \Gamma_q$ [13].

Table 1. Initial and boundary conditions.

Mechanical model		Hydraulic model	
$\mathbf{u}\left(\mathbf{X}, t\right) = \bar{\mathbf{u}}\left(t\right)$	$\mathbf{X} \in \Gamma_u$	$p\left(\mathbf{X}, t\right) = \bar{p}\left(t\right)$	$\mathbf{X} \in \Gamma_p$
$\boldsymbol{\sigma}\left(\mathbf{X}, t\right) \cdot \boldsymbol{\nu} = \bar{\mathbf{t}}\left(t\right)$	$\mathbf{X} \in \Gamma_t$	$\mathbf{q}\left(\mathbf{X}, t\right) \cdot \boldsymbol{\nu} = \bar{q}\left(t\right)$	$\mathbf{X} \in \Gamma_q$
$\mathbf{u}\left(\mathbf{X}, 0\right) = \mathbf{u}_0\left(\mathbf{X}\right)$		$p\left(\mathbf{X}, 0\right) = p_0\left(\mathbf{X}\right)$	

4 Modeling the discontinuity

The fracture propagation, associated with the non-linear behavior, is given by the following equations shown in Table 2.

Table 2. Fracture hydromechanical model.

$$
\boldsymbol{\Sigma}_{\Omega^h} = \begin{cases} \bar{\boldsymbol{\sigma}} & \text{if } \bar{\sigma}_{nn} \leqslant 0 \\ (1-d)\bar{\boldsymbol{\sigma}} & \text{if } \bar{\sigma}_{nn} > 0 \end{cases} \quad (6)
$$

$$
b_{\Omega^h} = 1 \quad (7)
$$

$$
\phi_{\Omega^h} = \phi_0 + \frac{[\![u]\!]_n}{h} \quad (9)
$$

$$
M_{\Omega^h} = \left(\frac{\phi_{\Omega^h}}{K_w}\right)^{-1} \quad (8)
$$

$$
\mathbf{k}_{\Omega^h} = \mathbf{k}_0 + \frac{[\![u]\!]_n^3}{f12h}\mathbf{s} \otimes \mathbf{s} \quad (10)
$$

The non-linear behavior of HAR-IEs is activated when the damage criterion is reached under tensile stresses according to eq. (6). The damage variable $d \in [0, 1]$ indicates that the material is intact ($d = 0$) or completely degraded ($d = 1$). Thus, once the damage criterion is satisfied in each HAR-IE causing their degradation, the creation of singularities at the fracture tip is avoided. The eq. (7) and eq. (8), which associated with the effective stress and the Biot's modulus constitutive model, respectively, define the parameters of the discontinuity. The eq. (9) presents the voids created due to fracture formation. The tangential flow variation is included in eq. (10) following the classical cubic law [18]. Note that the parameter h in eq. (9) and eq. (10) ensures a enrichment for the permeability and porosity composites [13].

For the stresses in the elastic domain, the damage criterion can be written as $\bar{\sigma}_{nn} - \varphi \leqslant 0$, where $\bar{\sigma}_{nn}$ is the component of the effective elastic stress tensor normal to the base of the HAR-IE and φ represents the size of the elastic domain in the space of elastic that assumes the highest value between f_t and $\bar{\sigma}_{nn}(\tau)$, where f_t is the porous media tensile strength. The damage variable can be written according to a softening parameter $\mathscr{A}$ [16] as follows:

$$
d = 1 - \frac{f_t}{\varphi} \exp\left[\mathscr{A}\left(1 - \frac{\varphi}{f_t}\right)\right]. \quad (11)
$$

It is important to remark that a fully coupled solution method is used to solve the governing equations using the Newton-Raphson method, in addition to using the IMPL-EX algorithm for integrating and solving the damage model. More details can be found at Manzoli et al. [13] and Cleto et al. [16].

5 Results

The simulations consider the geometry shown in Fig. 3(a) for a porous medium without NFs (Fig. 3(b)) and with a network of NFs (Fig. 3(d)). The porous medium has Young's modulus $E = 17.0$ GPa, tensile strength $f_t = 1.25$ MPa, fracture energy $G_f = 120.0$ N/m, Biot's coefficient $b = 0.75$, Biot's modulus $M = 68.7$ GPa, porosity $\phi_0 = 0.20$ and Poisson's ratio of $\nu = 0.2$. The stress state is isotropic compression with $\sigma_x = \sigma_y = 3.70$ MPa. The fluid has density $\rho = 1000$ kg/m^3, is incompressible Newtonian and injected into the well (Fig. 3(c)) with a constant injection rate for Case 1 with $Q_1 = 1.0 \times 10^{-3}$ kg/s and Case 2 with $Q_2 = 1.0$ kg/s. The NFs have apertures of 0.1 mm and 0.8 mm. Gravity was disregarded.

5.1 Case 1

The scenarios consider the porous medium without NFs, as well as the presence of a network of NFs for injection rate $Q_1 = 1.0 \times 10^{-3}$ kg/s. The pressure field for the porous medium without NFs (Fig. 4(a)) shows the
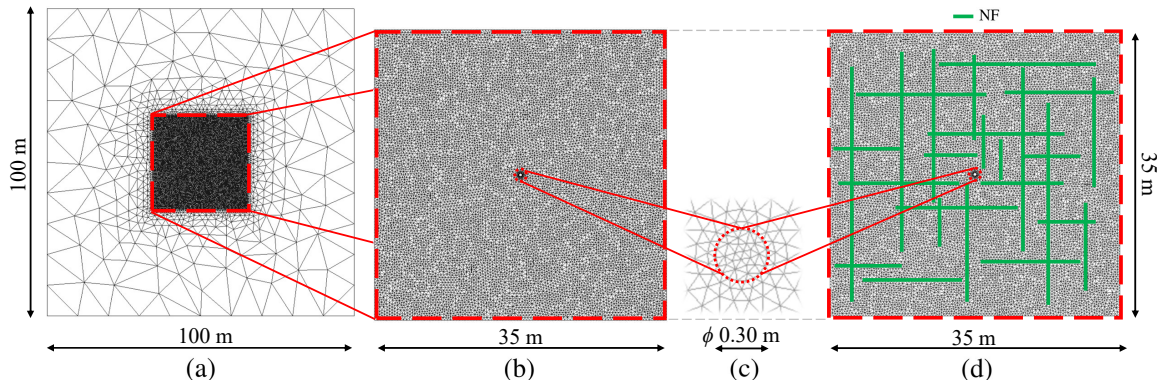
Figure 3. Geometry of the (a) regular mesh, (b) fragmented region, (c) well and (d) indication of the NFs.

propagation of an upper and lower branch of the HF, both symmetrically distanced from the well. However, note that only the upper branch is propagated preferentially. The pressure fields with NFs with apertures of 0.1 mm and 0.8 mm (Fig. 4(b) and Fig. 4(c), respectively) show that the HFs have two propagation branches and that they are deflected towards the NFs, which undergo changes in their respective pressure fields and become part of the fracturing of the porous medium. This behavior shows that one of the HF branches, on reaching the NF, is arrested by the NF, inducing the propagation of the other HF branch.

Note that the presence of NFs has a direct impact on the pressure fields, which contribute to the expansion of the fluid in the porous medium. This behavior intensifies as the NFs apertures increase, with the smaller apertures contributing more easily to leakage through the porous medium, while the larger apertures leak through the fracture walls. In this respect, in Fig. 4(b)-(c) it is possible to observe that the higher leakage of fluid through the NFs delays the advance of the HFs compared to the case without NFs, making it difficult for it to reach a longer extension.

5.2 Case 2

The pressure fields for the injection rate $Q_2 = 1.0$ kg/s are shown in Fig. 4(d)-(f). The field for the porous medium without NFs (Fig. 4(d)) shows a higher pressure variation, where two preferential HF propagation branches are obtained against only one observed in Case 1. Considering the presence of NFs (Fig. 4(e) and Fig. 4(f), respectively), three HF branches are observed. Note that the HFs tend to cross the NFs with smaller apertures directly and cross them with a offset to those with larger apertures, deflecting the direction of propagation of the HFs more easily to follow along the length of the NFs themselves.

Observe that the regions around the NFs undergo a less significant change compared to Case 1, indicating the trend that a higher fluid injection rate allows the fluid to quickly reach the porous medium through the HFs, but does not have enough time to leak through the fracture walls as before. In this respect, note that for Case 1 (Fig. 4(c)), all the NFs and their surroundings are affected by the fluid filling, but only the HF propagation region shows the greatest pressure changes (i.e. region with the highest fluid concentration). On the other hand, Case 2 (Fig. 4(f)) shows that all the interconnected NFs, as well as the HF propagation paths, suffered an intense impact on pressure to the detriment of the surroundings of all the NFs.

5.3 Pressure curves along time

The pressure-time curves for Case 1 and Case 2 are shown in Fig. 5(a) and (b), respectively. Note that the breakdown pressure (corresponding to the value required for fracture propagation to begin, given by the peak in the curve) is lower and takes longer to reach for Q_1 compared to Q_2.

Note that the impact of the NFs arresting the HF is captured by the pressure-time curves of Case 1 (Fig. 5(a)). The curve for NFs with apertures of 0.1 mm indicates a higher pressure compared to those of 0.8 mm, indicating more difficulty in filling the NFs with fluid. Comparing both curves with the case without NFs, it is possible to see that the HF arrested by the NFs produces an increase in pressure over time. Evaluating the curves for Case 2 (Fig. 5(b)), this behavior is not evident, showing that for a higher injection rate, the NFs have little influence. Note that only the curve for the larger-aperture NFs shows a slight difficulty in relief of pressure for $t \approx 18$ s. Thus, for a higher injection rate, the HFs were slightly affected by the larger aperture NFs.
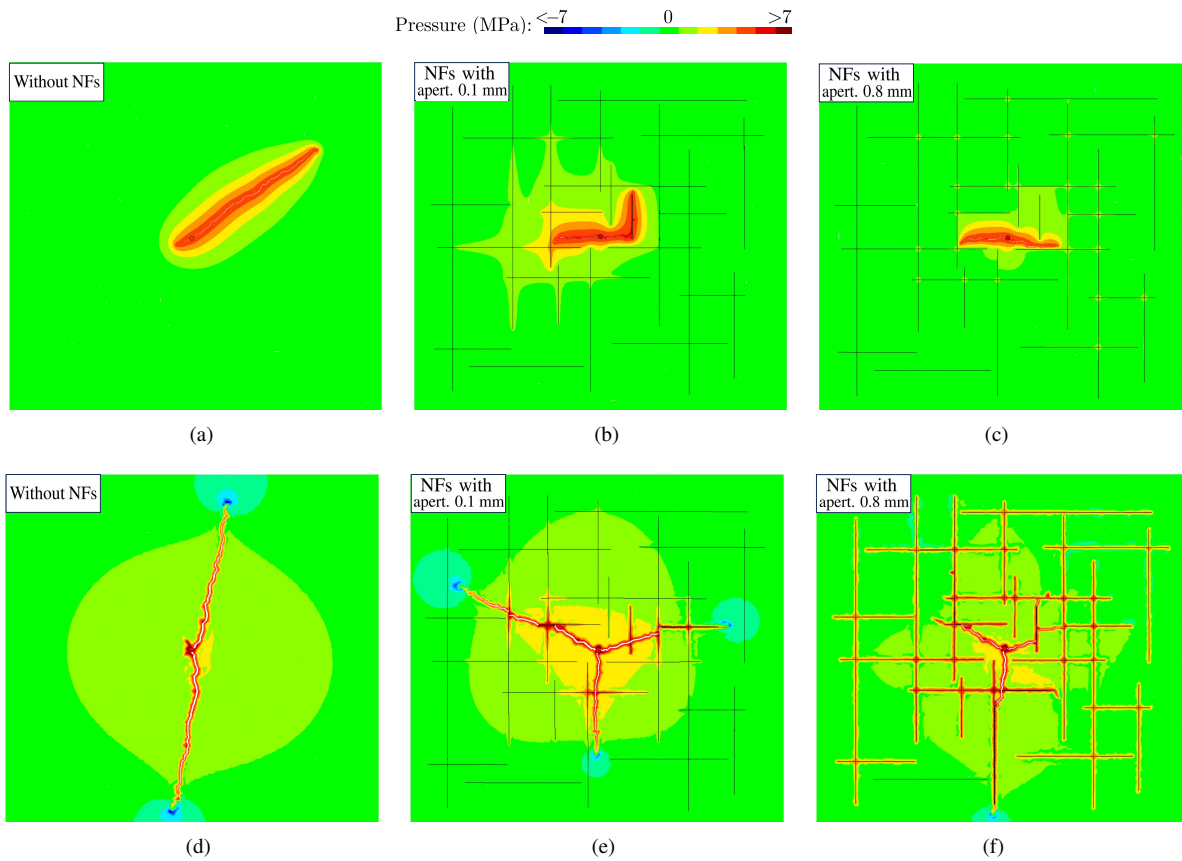
Figure 4. Pressure fields for the porous medium with Q_1 and (a) without NFs and with NFs aperture (b) 0.1 mm and (c) 0.8 mm for $t = 7500$ s. For Q_2, porous medium (d) without NFs and with NFs aperture (e) 0.1 mm and (f) 0.8 mm for $t = 40$ s. Deformation amplified 50x.
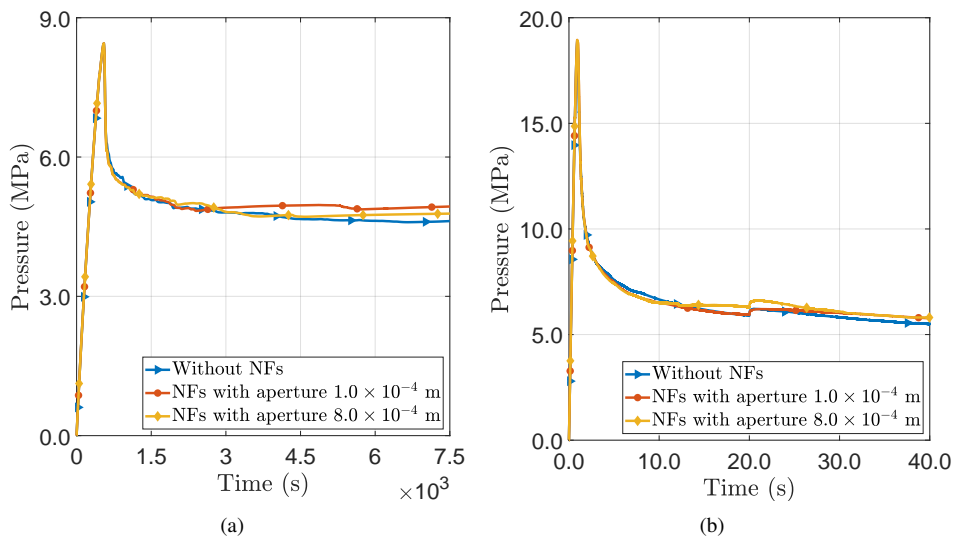
Figure 5. Pressure curves of the well along time for (a) Case 1 and (b) Case 2.

6 Conclusions

Hydraulic fracturing in naturally fractured porous media presents major differences compared to media without NFs. The distribution of the NFs considered in this study, most of them interconnected, shows how they tend

to facilitate fluid leakage, especially for a low injection rate. In addition, they require a much longer injection time for the HF to advance when compared to a higher injection case. The aperture of the NFs also has an impact on hydraulic fracturing, where larger apertures can make it easier for the HF to be arrested, deflecting the propagation.

The pressure-time curves capture the moment of encounter between fractures, an effect that was more evident for the case with a lower fluid injection rate. Thus, the moment of encounter between fractures, with the NFs arresting the HFs, leads to an increase in pressure due to the accumulation of fluid in the fractures. However, in the case with a higher injection rate, the NFs showed a slight impact on the curves, reflecting the low fluid filling and the increased advance of the HF. Thus, increasing the injection rate tends to reduce the influence of NFs.

Authorship statement. The authors hereby confirm that they are the sole liable persons responsible for the authorship of this work, and that all material that has been herein included as part of the present paper is either the property (and authorship) of the authors, or has the permission of the owners to be included here.

References

[1] J. Adachi, E. Siebrits, A. Peirce, and J. Desroches. Computer simulation of hydraulic fractures. *International Journal of Rock Mechanics and Mining Sciences*, vol. 44, n. 5, pp. 739 – 757, 2007.

[2] Q. He, F. T. Suorineni, and J. Oh. Review of hydraulic fracturing for preconditioning in cave mining. *Rock Mechanics and Rock Engineering*, vol. 49, n. 12, pp. 4893–4910, 2016.

[3] S. Kristianovitch and Y. Zheltov. Formation of vertical fractures by means of highly viscous fluids. In *Proceedings of the 4th World Petroleum Congress*, volume 2, pp. 579, 1955.

[4] J. Geertsma and F. De Klerk. Rapid method of predicting width and extent of hydraulically induced fractures. *Journal of Petroleum Technology;(United States)*, vol. 21, 1969.

[5] T. Perkins and L. Kern. Widths of hydraulic fractures. *Journal of Pet. Tech.*, vol. 13, n. 09, pp. 937–949, 1961.

[6] E. Bakhshi, N. Golsanami, and L. Chen. Numerical modeling and lattice method for characterizing hydraulic fracture propagation: A review of the numerical, experimental, and field studies. *Archives of Computational Methods in Engineering*, vol. 28, 2021.

[7] O. Kolawole and I. Ispas. Interaction between hydraulic fractures and natural fractures: current status and prospective directions. *Journal of Petroleum Exploration and Production Technology*, vol. 10, 2020.

[8] van D. B. Dam and de C. J. Pater. Roughness of hydraulic fractures: Importance of in-situ stress and tip processes. *SPE Journal*, 2001.

[9] L. N. Germanovich, R. S. Hurt, J. A. Ayoub, E. Siebrits, W. D. Norman, I. Ispas, and C. Montgomery. Experimental study of hydraulic fracturing in unconsolidated materials. *SPE International Conference and Exhibition on Formation Damage Control*, 2012.

[10] Y. Zou, S. Zhang, X. Ma, T. Zhou, and B. Zeng. Numerical investigation of hydraulic fracture network propagation in naturally fractured shale formations. *Journal of Structural Geology*, vol. 84, pp. 1–13, 2016.

[11] H. Wang. Hydraulic fracture propagation in naturally fractured reservoirs: Complex fracture or fracture networks. *Journal of Natural Gas Science and Engineering*, vol. 68, 2019.

[12] X. Wang, J. Chen, D. Ren, and J. Zhu. Role of natural fractures with topology structure for hydraulic fracture propagation in continental shale reservoir. *Engineering Fracture Mechanics*, vol. 284, pp. 109237, 2023.

[13] O. L. Manzoli, P. R. Cleto, M. Sánchez, L. J. Guimarães, and M. A. Maedo. On the use of high aspect ratio finite elements to model hydraulic fracturing in deformable porous media. *Computer Methods in Applied Mechanics and Engineering*, vol. 350, pp. 57 – 80, 2019.

[14] O. Manzoli, A. Gamino, E. Rodrigues, and G. Claro. Modeling of interfaces in two-dimensional problems using solid finite elements with high aspect ratio. *Computers & Structures*, vol. 94-95, pp. 70 – 82, 2012.

[15] J. Oliver. Modelling strong discontinuities in solid mechanics via strain softening constitutive equations. part 1: Fundamentals. *Int. journal for num. meth. in eng.*, vol. 39, n. 21, pp. 3575–3600, 1996.

[16] P. R. Cleto, M. Camargo, M. A. Maedo, E. A. Rodrigues, and O. L. Manzoli. Three-dimensional high aspect ratio interface elements for simulating 3d hydraulic fracturing in deformable porous media. *Computers & Structures*, vol. 283, 2023.

[17] O. L. Manzoli, M. A. Maedo, L. A. B. Jr., and E. A. Rodrigues. On the use of finite elements with a high aspect ratio for modeling cracks in quasi-brittle materials. *Eng. Frac. Mech.*, vol. 153, pp. 151 – 170, 2016.

[18] D. T. Snow. *A parallel plate model of fractured permeable media*. PhD thesis, University of California, 1965.